Nuclear Instruments and Methods in Physics Research A 742 (2014) 165–168

Contents lists available at ScienceDirect

Nuclear Instruments and Methods in Physics Research A

journal homepage: www.elsevier.com/locate/nima

Lorentz invariance violation: The latest Fermi results and the GRB/ AGN complementarity

J. Bolmont [a,*], V. Vasileiou [b], A. Jacholkowska [a], F. Piron [b], C. Couturier [a], J. Granot [c], F.W. Stecker [d], J. Cohen-Tanugi [b], F. Longo [e]

[a] LPNHE, Université Pierre et Marie Curie Paris 6, Université Denis Diderot Paris 7, CNRS/IN2P3, France
[b] LUPM, Université Montpellier 2, CNRS/IN2P3, France
[c] Department of Natural Sciences, The Open University of Israel, Israel
[d] Astrophysics Science Division, NASA/Goddard Space Flight Center and Department of Physics and Astronomy, University of California, USA
[e] Istituto Nazionale di Fisica Nucleare, Sezione di Trieste and Dipartimento di Fisica, Università di Trieste, Italy

ARTICLE INFO

Available online 6 November 2013

Keywords:
Quantum gravity
Lorentz invariance violation
Fermi-LAT
Gamma-ray burst

ABSTRACT

Because they are bright and distant, Gamma-ray Bursts (GRBs) have been used for more than a decade to test propagation of photons and to constrain relevant Quantum Gravity (QG) models in which the velocity of photons in vacuum can depend on their energy. With its unprecedented sensitivity and energy coverage, the *Fermi* satellite has provided the most constraining results on the QG energy scale so far. In this talk, the latest results obtained from the analysis of four bright GRBs observed by the Large Area Telescope will be reviewed. These robust results, cross-checked using three different analysis techniques set the limit on QG energy scale at $E_{QG,1} > 7.6$ times the Planck energy for linear dispersion and $E_{QG,2} > 1.3 \times 10^{11}$ GeV for quadratic dispersion (95% CL). After describing the data and the analysis techniques in use, results will be discussed and confronted to latest constraints obtained with Active Galactic Nuclei.

1. Introduction

The most followed approach for experimental search of Quantum Gravity (QG) is probably to test Lorentz Invariance Violation (LIV) [1–3]. A very generic and model-independent formalism to achieve this goal consists in writing the dispersion relations as a series expansion of the form

$$E^2 \simeq p^2c^2 \times \left[1 - \sum_{n=1}^{\infty} s_{\pm} \left(\frac{E}{E_{QG}}\right)^n\right] \quad (1)$$

where c is the low energy limit of the speed of light, $s_{\pm}$ allows to take into account subluminal ($s_{\pm} = +1$) and superluminal ($s_{\pm} = -1$) propagations and E_{QG} is the energy scale at which the LIV effects become important. The goal of LIV searches is to put constrains on $E_{QG,n}$ measuring the time lag between photons of different energies produced by distant sources such as Gamma-ray Bursts (GRB) or TeV flares from Active Galactic Nuclei (AGN), assuming these photons have been emitted at the same time. Since E_{QG} is much higher than the energy of all gamma-ray photons observed, the lowest order term dominates in Eq. (1). At present day, only the $n=1$ and $n=2$ orders can be constrained with good sensitivity.

When two photons are emitted at redshift z with an energy difference of $\Delta E^n = E_h^n - E_l^n$, Eq. (1) leads to the following expression for the time delay Δt between the two photons at their arrival to the detector:

$$\tau_n \equiv \frac{\Delta t}{\Delta E} \simeq s_{\pm} \frac{(1+n)}{2H_0} \frac{1}{E_{QG,n}^n} \times \kappa_n \quad (2)$$

where

$$\kappa_n \equiv \int_0^z \frac{(1+z')^n}{\sqrt{\Omega_\Lambda + \Omega_M (1+z')^3}} dz' \quad (3)$$

is the comoving distance between the source and the observer, z is the redshift, $H_0 = 73.8 \pm 2.4$ km s^{-1} Mpc^{-1} [4] is the Hubble constant and $\Omega_\Lambda = 0.728$ and $\Omega_M = 0.272$ the cosmological constant and the total matter density as measured by WMAP in the framework of the ΛCDM model [5].

The Large Area Telescope (LAT) on board the *Fermi* satellite has provided the most constraining limits on $E_{QG,n}$ so far, obtained using GRBs 080916C [6] and 090510 [7]. These past results were derived by studying the highest energy photon detected in coincidence with the bursts or using the DisCan method [13] in the case of GRB 090510. In this note, four bright bursts of known redshifts are studied with three different statistical methods which allow us to obtain even stronger and more robust limits.

* Corresponding author. Tel.: +33 14427 4818.
E-mail address: bolmont@in2p3.fr (J. Bolmont).

0168-9002/$ - see front matter © 2013 Elsevier B.V. All rights reserved.
http://dx.doi.org/10.1016/j.nima.2013.10.088

In the next section, the latest analysis of four bright GRBs observed by Fermi-LAT will be described [8]. This work has been carried out with the goal to be as complete as possible: the results were given for both subluminal and superluminal propagations and include also the limits expressed in the SME framework of Kostelecký and Mewes [9]. In this proceeding, we will only describe the key points of the analysis (Section 2) and discuss a subset of the results (Section 3). In Section 4, we will conclude and put the results in context with other constraints obtained with AGNs.

2. Analysis of four bright bursts observed by Fermi-LAT

2.1. The data

The four GRB analyzed have a bright GeV prompt emission and a measured redshift. These GRBs are 080916C, 090510, 090902B and 090926A, located respectively at $z = 4.35 \pm 0.15$, 0.903 ± 0.003, 1.822 and 2.107. The LAT events passing the P7_TRANSIENT_V6 selection are considered in the analysis, only excluding events with reconstructed energies lower than 30 MeV because of their limited energy and angular reconstruction precisions. The events reconstructed in a circular region of interest (ROI) of radius 12° centered on the GRB position are kept to limit the number of background or poorly reconstructed events included in the analysis.

In addition to these cuts, a time selection is applied in order to analyze the data where the temporal variability is maximized. Time intervals are used to limit the effect of spectral variability that can happen during the burst and could mimic a LIV-dispersion effect. These intervals were determined for each burst, for $n=1$ and $n=2$, taking into account the possible LIV dispersion effect, ensuring that no photon that was out of the interval at the source is detected in the interval, and vice versa. The degree of LIV dispersion used for time interval selection corresponds to the conservative values of $E_{\mathrm{QG},1} = 0.5 \times E_{\mathrm{Pl}}$ and $E_{\mathrm{QG},2} = 1.5 \times 10^{10}$ GeV.

2.2. Methods in use

The goal of the analysis is to measure the level of dispersion τ_n present in the data. For this, we used three different methods, applied on the data passing the selections described in the previous section. The first two methods were developed for this work, while the third (likelihood) has been used already in LIV searches [10,11] and will not be described further in this paper.

For each method, confidence intervals (CI) on the LIV parameter estimates were determined using toy Monte Carlo techniques (see [8] for details).

2.2.1. PairView

The PairView (PV) method calculates the spectral lags $l_{i,j}$ between all pairs of photons in a data set and uses the distribution of their values to estimate the LIV parameter. For a data set consisting of N photons with detection times $t_{1\ldots N}$ and energies $E_{1\ldots N}$, the method starts by calculating the $N \times (N-1)/2$ photon-pair spectral lags $l_{i,j}$ for each $i > j$:

$$l_{i,j} \equiv \frac{t_i - t_j}{E_i^n - E_j^n} \tag{4}$$

(where n is the order of LIV), and creates a distribution of their values. Such a distribution is shown by Fig. 1 (top) in the case of GRB 090510. The estimator $\hat{\tau}_n$ of τ_n is taken as the location of the maximum of the $l_{i,j}$ distribution. To find the maximum of the distribution in the most unbiased way possible, a kernel density estimate (KDE, [12]) is used on unbinned data.

2.2.2. Sharpness-Maximization Method

The Sharpness-Maximization Method (SMM) uses the fact that any form of spectral dispersion applied to the data would smear the light curve decreasing its sharpness. The level of dispersion present in the data, is the one that maximizes the sharpness of the light curve when it is removed from the data. This procedure is based on the DisCan method previously used on *Fermi* data [13].

To remove a LIV dispersion from the data consisting of photons with time and energies (t_i, E_i), we subtract $E_i^n \times \tau_n$ from the detection time t_i. then the sharpness is computed according to

$$\mathcal{S}(\tau_n) = \sum_{i=1}^{N-\rho} \log\left(\frac{\rho}{t'_{i+\rho} - t'_i}\right) \tag{5}$$

where ρ is a configurable parameter of the method. Repeating this operation with different values of τ_n allows us to extract the best estimate of $\hat{\tau}_n$ for which the sharpness is maximized. Fig. 1 (center) shows the sharpness measured in the case of GRB 090510 for a parameter τ_1 varying from -0.1 to 0.1 s/GeV. For completeness, Fig. 1 (right) shows the likelihood curve obtained with the same GRB.

The parameter ρ was chosen for each GRB by applying the method on several thousands of simulated datasets inspired by the GRB under study. The value chosen for ρ is the one that gives the most constraining median upper limit on τ_n (for $s_\pm = +1$).

2.3. Results

The lags measured with the three methods (PV, SMM and likelihood) are given by Fig. 2 together with the 90% and 95% (two-sided) confidence intervals. No evidence is seen for a variation of τ_n with κ_n as would be expected for a LIV effect. In addition, all measured lags are compatible with zero and the three methods are in good agreement with each other.

From the constraints obtained on τ_n, it is possible to derive lower limits on $E_{\mathrm{QG,n}}$. Fig. 3 shows these limits as a function of the redshift. In some cases, the CIs have edges that fall very close to zero as can be seen in Fig. 2. These intervals give spuriously stringent upper limits or even limits that cannot be computed at all. In these cases, we interpret the lags as being due to GRB intrinsic spectral-evolution effects.

GRB intrinsic effects are due to the evolution of the emitted spectrum during the GRB: photons with different energies can preferentially be emitted at different times. The measured lag τ_n is actually the sum of intrinsic lags τ_{int} and those due to LIV τ_{LIV}. In order to evaluate their impact on our results, we modeled the intrinsic lags assuming that our constraints on τ_n also apply on τ_{int} and that τ_{int} is null on average. Assuming the range of possible values for τ_{int} is the same as for τ_n, and considering the less constraining results, we were able to produce a new set of limits. These conservative limits (the bars shown on Fig. 3) are much weaker than the ones obtained using τ_n only.

The intrinsic effects are the main source of systematics in the present study. Other systematics, due to the instrument response and the error on redshift and cosmological parameters, can be neglected.

3. Comparison of GRB and AGN constraints

Many constraints have been obtained in the past on $E_{\mathrm{QG},1}$ and $E_{\mathrm{QG},2}$ using observations of GRBs by satellites on the one hand and observations of AGNs by ground-based Cherenkov detectors on the other hand (see e.g. [14] for a review). Three comments can be made:

- For GRBs, a large amount of data are available from satellites. No GRB has been seen by ground-based experiments so far. Satellites can detect photons up to a few hundred GeVs. At these energies, very distant GRBs can be detected, since the

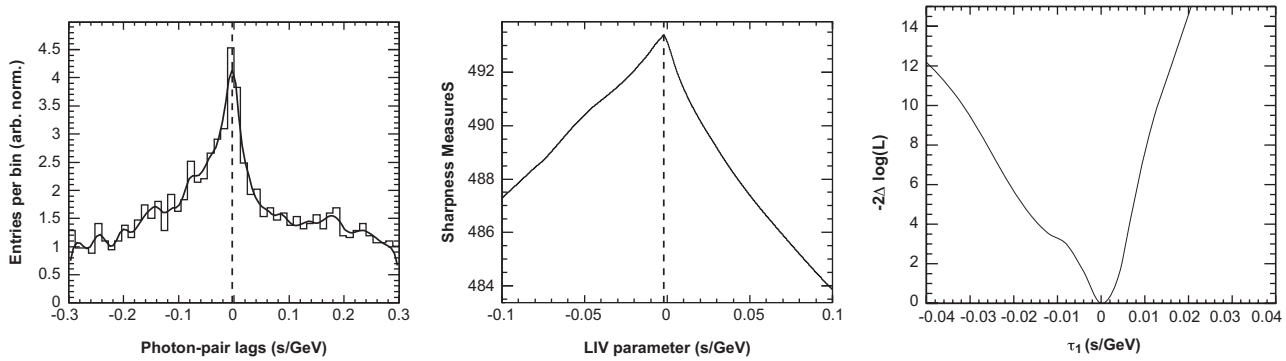

Fig. 1. Application of the three methods to the same dataset (GRB 090510) and for a linear LIV. Left: PairView. Distribution of the l_{ij} parameters (Eq. (4)). The best estimate for τ_1 is given by the maximum of the KDE (black curve) of the histogram. Center: SMM. The curve shows the evolution of parameter $\mathcal{S}(\tau_1)$. Right: Likelihood. The best estimate is the value which minimizes the value of $-2\Delta\log(\mathcal{L})$, where $\mathcal{L}$ is the likelihood to observe an event of energy E at time t taking into account a time lag τ_1.

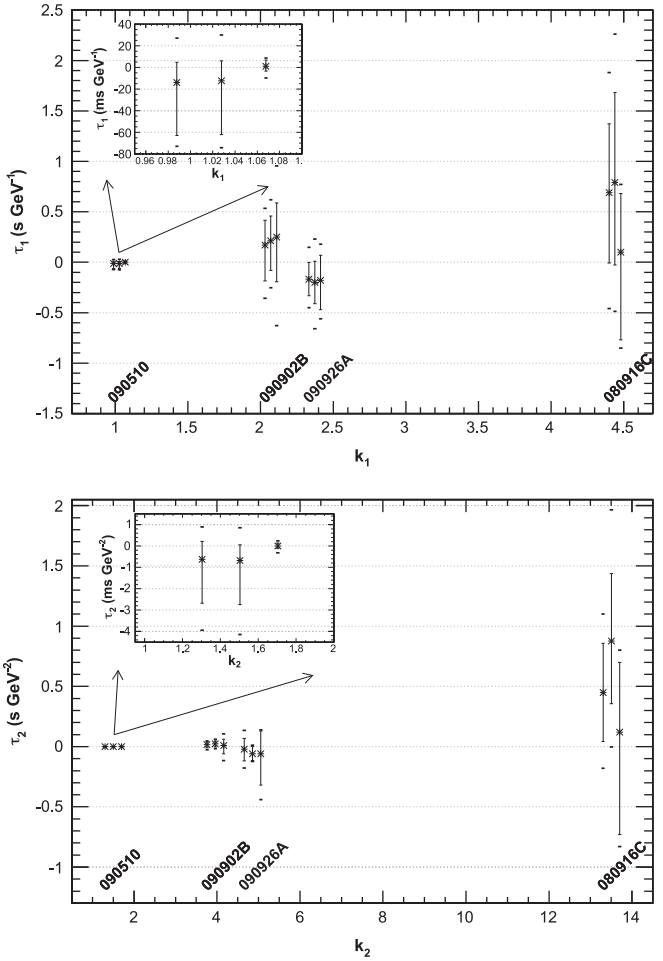

Fig. 2. Confidence intervals obtained for the four GRBs and the three methods on the total amount of dispersion in the data τ_n. Top linear LIV, bottom: quadratic LIV. The horizontal axis corresponds to the distance parameter κ_n (Eq. (3)). Each group of three points corresponds to one GRB with (top to bottom) PV, SMM and ML. The points have been separated to improve readability. The error bars correspond to 90% (two-sided) CL and the pairs of points to 99% (two-sided) CL.

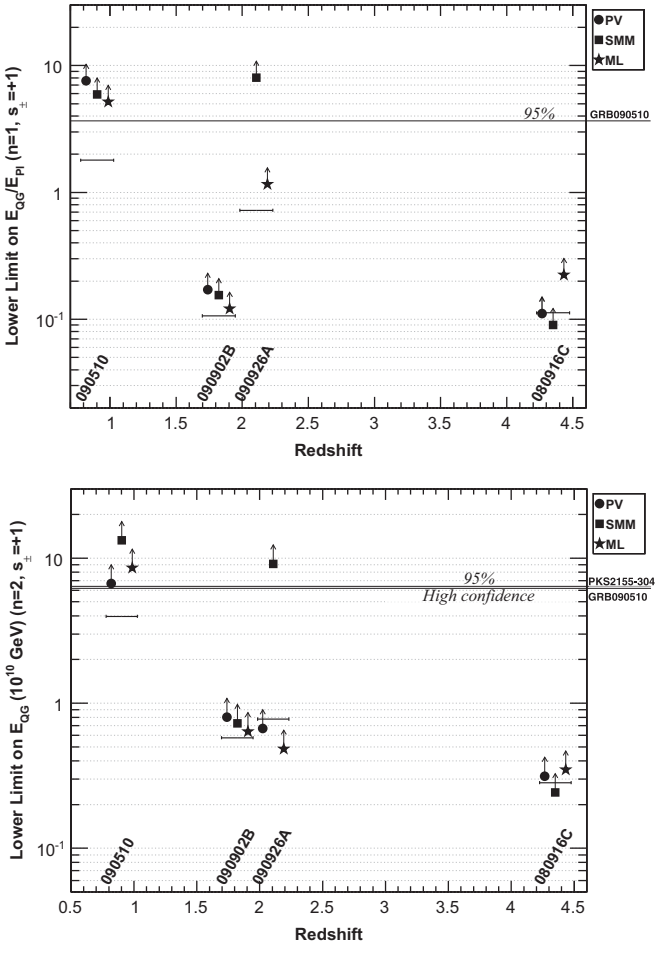

Fig. 3. 95% one-sided lower limits obtained on $E_{\mathrm{QG,n}}$ for linear (top) and quadratic LIV (bottom) for the subluminal case. Each group of three points corresponds to one GRB with (top to bottom) PV, SMM and ML. The points have been separated to improve readability. The horizontal bars give the limits obtained averaging over the three methods and taking into account the source-intrinsic effects.

photons are only weakly absorbed by the Extragalactic Background Light (EBL, [15]).

- For AGNs observed by ground-based experiments, not only a detection is necessary, but also a significant variability is needed. This condition, added to the fact that a redshift measurement is also needed, has led to the fact that only three AGNs were analyzed so far to search for LIV. AGNs are seen by space-based experiments, but with low statistics due to their limited effective area. Ground-based Cherenkov telescopes have an energy range going from a few hundred GeVs to a few TeVs. At these energies, only nearby sources can be detected because of the EBL absorption.
- GRBs and AGNs have different origins and therefore do not have a priori the same intrinsic effects. For the moment, there is no fully accepted model to explain both spectral properties and flux evolution in time, either for GRBs or for AGNs.

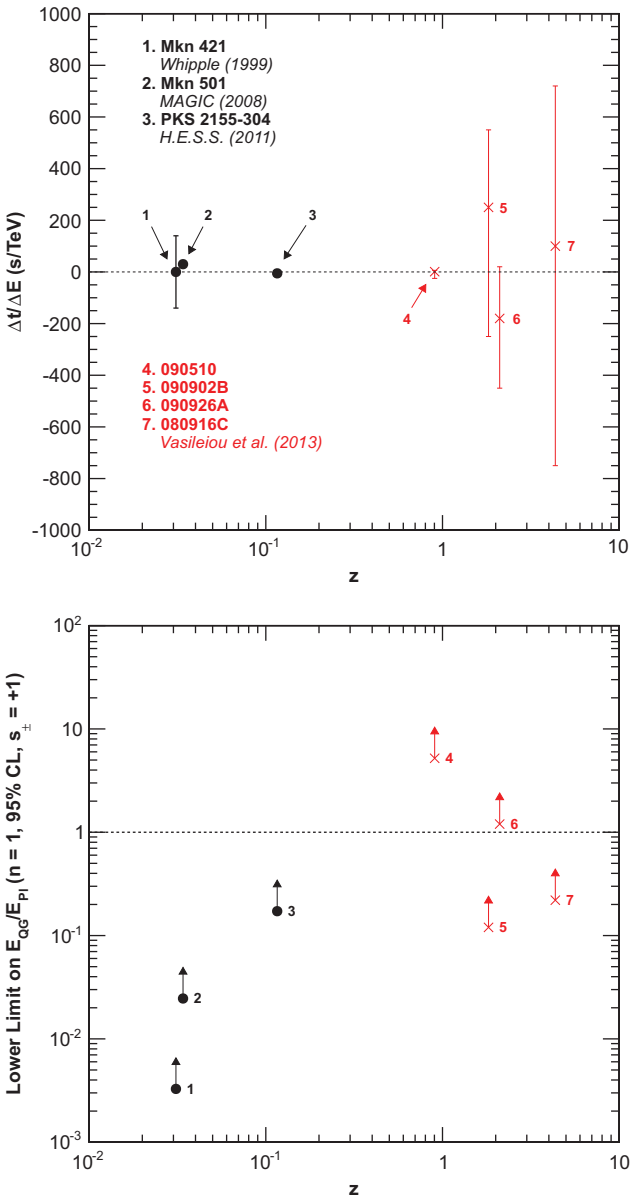

Fig. 4. Spectral lags (top) and the corresponding lower limits on $E_{QG,1}$ (bottom) obtained in [8] (red crosses) and in previous works (black dots) using AGN high energy gamma-ray observations: (1) *Whipple* observation of Mkn 421 [16]; (2) MAGIC observation of Mkn 501 [10]; (3) H.E.S.S. observation of PKS 2155-304 [11]. See the text for comments. (For interpretation of the references to color in this figure caption, the reader is referred to the web version of this article.)

For these reasons, it is necessary to study both GRBs and AGNs to look for LIV.

Fig. 4 allows us to compare the results obtained in the present study with previous ones obtained with AGNs. All these results were obtained using a ML method and all correspond to a subluminal propagation. The furthest AGN in this plot is PKS 2155-304, with $z=0.116$ while the most distant GRB is 080916C. On the top plot, the error bars are smaller for AGNs than for GRBs. That is a direct consequence of the fact the energy lever arm (related to the parameter ΔE in Eq. (2) and therefore to the energy coverage of the instruments) is much larger in ground-based observations. On the plot on the top, one can see that the limits obtained with AGNs are on average less constraining than those obtained with GRBs. However, a giant flare as the one of PKS 2155-304 in 2006 gives a constraint which is at the level of some GRBs with higher redshifts. Finally, we have to point out that GRB 090510 can be considered as peculiar in a sense that it is very short, very bright and very energetic.

4. Conclusions

Using three different analysis techniques to analyze *Fermi*-LAT data, we were able to set the best limits so far for linear and quadratic LIV. These limits are obtained with GRB 090510, namely $E_{QG,1} > 7.6\, E_{Pl}$ (PV) and $E_{QG,2} > 1.3 \times 10^{11}$ GeV (SMM). These results are a factor of ~ 2 better than the previous results from *Fermi* and H.E.S.S. and they disfavor any class of models requiring $E_{QG,1} \lesssim E_{Pl}$.

Not many AGNs and GRBs have been detected with the properties of PKS 2155-304 or those of 090510 and a lot has to be done to improve emission models and our understanding of intrinsic effects. A future instrument like CTA [17] will have a dedicated survey pointing mode which will greatly improve its sensitivity to transient sources, GRBs and flaring AGNs included. Population studies involving both kinds of sources will then be possible, further constraining the models of linear and quadratic LIV.

Acknowledgments

The *Fermi* LAT Collaboration acknowledges support from a number of agencies and institutes for both development and the operation of the LAT as well as scientific data analysis. These include NASA and DOE in the United States, CEA/Irfu and IN2P3/CNRS in France, ASI and INFN in Italy, MEXT, KEK, and JAXA in Japan, and the K. A. Wallenberg Foundation, the Swedish Research Council and the National Space Board in Sweden. Additional support from INAF in Italy and CNES in France for science analysis during the operations phase is also gratefully acknowledged.

References

[1] L. Smolin, Three Roads to Quantum Gravity, Basic Books, New York, 2001.
[2] D. Mattingly, Liv. Rev. Relativ. 11 (2005) 5.
[3] T. Jacobson, S. Liberati, D. Mattingly, Ann. Phys. 321 (2006) 150.
[4] A.G. Riess, et al., Astrophys. J. 730 (2011) 119.
[5] E. Komatsu, et al., Astrophys. J. Suppl. Ser. 192 (2011) 18.
[6] A.A. Abdo, et al., Science 323 (2009) 1688.
[7] A.A. Abdo, et al., Nature (London) 462 (2009) 331.
[8] V. Vasileiou, et al., Phys. Rev. D 87 (2013) 122001 arxiv:1305.3463.
[9] V.A. Kostelecký, M. Mewes, Phys. Rev. D 80 (2009) 015020.
[10] M. Martinez, M. Errando, Astropart. Phys. 31 (2009) 226.
[11] A. Abramowski, et al., H.E.S.S. Collaboration, Astropart. Phys. 34 (2011) 738.
[12] K.S. Cranmer, Comp. Phys. Com. 136 (2001) 198.
[13] J.D. Scargle, et al., Astrophys. J. 673 (2008) 972.
[14] J. Bolmont, A. Jacholkowska, ASR 47 (2011) 380.
[15] E. Dwek, F. Krennrich, Astropart. Phys. 43 (2013) 112.
[16] S.D. Biller, et al., Whipple Collaboration, Phys. Rev. Lett. 83 (1999) 2108.
[17] The CTA Consortium, Exp. Astron. 32 (2011) 193.